Conformational changes in the catalytically inactive nucleotide-binding site of CFTR

László Csanády,[1,2] Csaba Mihályi,[1] Andras Szollosi,[1] Beáta Töröcsik,[1] and Paola Vergani[3]

[1]Department of Medical Biochemistry and [2]MTA-SE Ion Channel Research Group, Semmelweis University,
Budapest H-1094, Hungary
[3]Department of Neuroscience, Physiology and Pharmacology, University College London, London WC1E 6BT, England, UK

A central step in the gating of the cystic fibrosis transmembrane conductance regulator (CFTR) chloride channel is the association of its two cytosolic nucleotide-binding domains (NBDs) into a head-to-tail dimer, with two nucleotides bound at the interface. Channel opening and closing, respectively, are coupled to formation and disruption of this tight NBD dimer. CFTR is an asymmetric adenosine triphosphate (ATP)-binding cassette protein in which the two interfacial-binding sites (composite sites 1 and 2) are functionally different. During gating, the canonical, catalytically active nucleotide-binding site (site 2) cycles between dimerized prehydrolytic (state O_1), dimerized post-hydrolytic (state O_2), and dissociated (state C) forms in a preferential $C \rightarrow O_1 \rightarrow O_2 \rightarrow C$ sequence. In contrast, the catalytically inactive nucleotide-binding site (site 1) is believed to remain associated, ATP-bound, for several gating cycles. Here, we have examined the possibility of conformational changes in site 1 during gating, by studying gating effects of perturbations in site 1.

Previous work showed that channel closure is slowed, both under hydrolytic and nonhydrolytic conditions, by occupancy of site 1 by N^6-(2-phenylethyl)-ATP (P-ATP) as well as by the site-1 mutation H1348A (NBD2 signature sequence). Here, we found that P-ATP prolongs wild-type (WT) CFTR burst durations by selectively slowing ($>2\times$) transition $O_1 \rightarrow O_2$ and decreases the nonhydrolytic closing rate (transition $O_1 \rightarrow C$) of CFTR mutants K1250A ($\sim4\times$) and E1371S ($\sim3\times$). Mutation H1348A also slowed ($\sim3\times$) the $O_1 \rightarrow O_2$ transition in the WT background and decreased the nonhydrolytic closing rate of both K1250A ($\sim3\times$) and E1371S ($\sim3\times$) background mutants. Neither P-ATP nor the H1348A mutation affected the 1:1 stoichiometry between ATP occlusion and channel burst events characteristic to WT CFTR gating in ATP. The marked effect that different structural perturbations at site 1 have on both steps $O_1 \rightarrow C$ and $O_1 \rightarrow O_2$ suggests that the overall conformational changes that CFTR undergoes upon opening and coincident with hydrolysis at the active site 2 include significant structural rearrangement at site 1.

INTRODUCTION

CFTR (ABCC7; Riordan et al., 1989) is a member of the asymmetric C subfamily of ATP-binding cassette (ABC) proteins. Most ABC proteins are active transporters that move a variety of substrates across biological membranes. The substrate translocation pathway, formed by two transmembrane domains (TMDs), cycles between inward- and outward-facing conformations driven by an ATP hydrolysis cycle catalyzed by the two cytosolic nucleotide-binding domains (NBDs). ABC NBDs contain three highly conserved sequence motifs: the Walker A (GXXXXGKS/T) and B (ΦΦΦΦDE, with Φ representing hydrophobic residues), and the ABC signature motif (LSGGQR/K). In each catalytic cycle, ATP binding to the Walker motifs of both NBDs promotes formation of a tight head-to-tail NBD dimer that occludes two ATP molecules in composite interfacial catalytic sites formed by the Walker motifs of one NBD and the signature motif

of the other. ATP hydrolysis is required to disrupt this dimer to allow nucleotide exchange and initiation of a new cycle (Hollenstein et al., 2007). Members of the C subfamily share this overall architecture but show a marked asymmetry in the primary sequences of their two NBDs. Because of noncanonical substitutions in the Walker B and in other conserved motifs of the N-terminal NBD (NBD1) and in the signature sequence of the C-terminal NBD (NBD2), the catalytic site containing these motifs (site 1) is inactive (Aleksandrov et al., 2002; Basso et al., 2003), leaving ABC-C proteins with a single catalytically active site (site 2, formed by Walker motifs of NBD2 and signature sequence of NBD1). Non-canonical substitutions in the same key positions, resulting in reduced or absent hydrolysis at one composite site, are also seen in the clinically important transporter associated with antigen processing (formed by TAP1 and TAP2 of the human ABC-B subfamily; Procko et al., 2009),

---

Correspondence to László Csanády:
csanady.laszlo@med.semmelweis-univ.hu

Abbreviations used in this paper: ABC, ATP-binding cassette; NBD, nucleotide-binding domain; P-ATP, N^6-(2-phenylethyl)-ATP; P_o, channel open probability; RI, regulatory insertion; TMD, transmembrane domain.

Supplemental Material can be found at:
http://jgp.rupress.org/content/suppl/2013/06/10/jgp.201210954.DC1.html

as well as in numerous yeast and prokaryotic transporters (Szollosi et al., 2011). The latter group includes TM287/288, a heterodimeric transporter from *Thermotoga maritima*, whose high resolution structure has been recently solved (Hohl et al., 2012).

CFTR, the protein mutated in cystic fibrosis patients (Riordan et al., 1989), is the only member of the ABC-C family whose TMDs are known to form the pore of a Cl⁻ ion channel. In addition to the canonical ABC domains, CFTR contains a unique regulatory (R) domain, phosphorylation of which by cAMP-dependent protein kinase (PKA) is a prerequisite for channel gating (Anderson et al., 1991). In phosphorylated CFTR, the pore opens to a burst upon ATP-induced dimerization of its NBDs and closes from a burst upon dimer dissociation (Vergani et al., 2005) after ATP hydrolysis at site 2; thus, in WT CFTR, each gating cycle (or burst of openings) is coupled to hydrolysis of one ATP molecule (Csanády et al., 2010). Deviations from this strict 1:1 coupling between ATP hydrolysis events and bursts of openings have been suggested to happen in mutants or in the presence of drugs. Catalytic site mutations can lower this coupling ratio leading to bursts that involve ATP occlusion/deocclusion but no hydrolysis (Csanády et al., 2010). In contrast, [ATP]-dependent prolongation of open burst durations for the W401F CFTR mutant (Jih et al., 2012b), or for WT CFTR gating in the presence of the potentiator compound Vx-770 (Jih and Hwang, 2013), has led to the suggestion that post-hydrolytic ADP/ATP exchange in site 2 might occur without intervening pore closure, thereby increasing the coupling ratio by allowing more than one ATP to be hydrolyzed in site 2 within a single gating cycle (Jih et al., 2012a).

Biochemical work using γ-³²P-labeled ATP analogues revealed that ATP remains bound at CFTR's NBD1 for periods much longer (several minutes) than a channel gating cycle (∼1 s), without being hydrolyzed (Aleksandrov et al., 2002; Basso et al., 2003). In a recent study (Tsai et al., 2010), nucleotide exchange time constants at the two sites were measured using a functional approach. The high affinity ATP analogue N^6-(2-phenylethyl)-ATP (P-ATP) was found to speed the opening and slow the closing of CFTR channels, but the onset of these two effects upon sudden replacement of ATP with P-ATP in the bath (cytosolic) solution followed distinct time courses. Whereas the effect on opening rate appeared instantaneously, suggesting that it was caused by P-ATP binding to the rapid-turnover site 2, the onset of slowed closure followed with a delay of 30–50 s, consistent with ATP/P-ATP exchange occurring more slowly at degenerate site 1. Furthermore, because the nucleotide exchange rate at site 1 was affected by mutations in the NBD2 signature sequence, which completes site 1 only in a formed dimer, the authors suggested only partial separation of the NBD dimer in closed channels, with the interface remaining closed around site 1 for several gating cycles. This notion obtained further support from thermodynamic studies (Szollosi et al., 2011) that examined state-dependent changes in energetic coupling between pairs of residues on opposing faces of the site-1 interface. A lack of change in energetic coupling for three such pairs was interpreted to be consistent with the model suggested by Tsai et al. (2010), i.e., with an "immobile" site 1 remaining closed throughout the gating cycle.

Nevertheless, site 1 clearly does play a role in gating energetics, as perturbations at site 1 can profoundly alter channel gating kinetics. For instance, the K464A mutation, which—by removing the side chain of the conserved NBD1 Walker A lysine—perturbs the NBD1 side of site 1, dramatically alters the mechanism of gating (Csanády et al., 2010). In addition, the H1348A mutation in the NBD2 signature sequence, which perturbs the NBD2 side of site 1, was found to slow channel closure (Szollosi et al., 2011). Finally, gating is affected by perturbations of the nucleotide structure at site 1, as P-ATP bound at site 1 also slows channel closure (Tsai et al., 2010). However, the exact mechanisms by which the H1348A mutation, or P-ATP bound at site 1, affects gating have not yet been elucidated. To gain further insight into the energetic consequences of perturbations at site 1, we examined in detail the effects of these two perturbations on CFTR channel gating. Our observations suggest that, despite maintained contact between residues on opposite sides of site 1, this site does not remain "frozen"; rather, significant conformational changes are likely to take place there both during channel opening and concomitant with ATP hydrolysis at site 2.

MATERIALS AND METHODS

Molecular biology
Human WT CFTR and CFTR segment 433–1480 in the pGEMHE plasmid (Chan et al., 2000) served as templates for mutants H1348A, K1250A, E1371S, K1250A/H1348A, E1371S/H1348A, E1371S/K464A, and 433–1480(K1250A), which were created using the QuikChange kit (Agilent Technologies). The entire coding sequence of each construct was verified by automated sequencing (LGC Genomics). T7 polymerase was used for in vitro transcription (Mmessage kit; Ambion), and purified cRNA was stored at −80°C.

Isolation and injection of *Xenopus laevis* oocytes
Xenopus oocytes were extracted and treated with collagenase as described previously (Chan et al., 2000). Isolated oocytes were stored at 18°C in a solution containing (mM) 82 NaCl, 2 KCl, 1 $MgCl_2$, 5 HEPES, pH 7.5 with NaOH, 1.8 $CaCl_2$, and 50 µg/ml gentamycin. To obtain expression levels appropriate for single-channel or macroscopic recordings, oocytes were microinjected with 0.1–10 ng of CFTR cRNA, and further incubated at 18°C for 2–3 d.

Excised inside-out patch-clamp recordings
For inside-out patch recordings, the pipette solution contained (mM) 136 NMDG-Cl, 2 $MgCl_2$, and 5 HEPES, pH 7.4 with NMDG.

The bath solution was continuously flowing and contained (mM) 134 NMDG-Cl, 2 MgCl$_2$, 5 HEPES, and 0.5 EGTA, pH 7.1 with NMDG. MgATP (Sigma-Aldrich) was added from a 400-mM aqueous stock solution (pH 7.1 with NMDG) to achieve a final concentration of 2 mM (or 10 mM for channels bearing the K1250A mutation). A 10-mM aqueous stock solution of P-ATP Na$^+$ salt (BIOLOG Life Science Institute) was stored at −80°C and diluted into the bath solution immediately before recording to achieve a final concentration of 10 µM (or 50 µM for K1250A mutants). CFTR channels were fully activated by a 1–2-min cytosolic exposure to 300 nM of catalytic subunit of PKA (Sigma-Aldrich); all experiments shown were done in the partially dephosphorylated state after PKA removal, which remains stable over the time course of several minutes (Csanády et al., 2000). Switching between various bath solutions was achieved using computer-controlled electronic valves (HEKA); solution exchange time constant was 20–50 ms. Experiments were performed at 25°C. Unitary CFTR currents were recorded (Axopatch 200B; Molecular Devices) at a pipette holding potential of +80 mV (V$_m$ = −80 mV), filtered at 2 kHz, and digitized at 10 kHz (Digidata 1322A, Pclamp9; Molecular Devices). As CFTR gating is largely voltage independent (Cai et al., 2003), macroscopic currents were recorded at membrane potentials between −20 and −80 mV.

Steady-state kinetic analysis of multichannel patches

Mean burst and interburst durations were extracted from steady segments of record with one to six active CFTR channels as described previously (Csanády et al., 2000). Currents were digitally filtered at 100 Hz and idealized by half-amplitude threshold crossing. Events lists were fitted with a simple model in which ATP-dependent slow gating is pooled into a closed-open scheme and ATP-independent brief closures are modeled as pore-blockage events (Ishihara and Welsh, 1997). Rate constants (r_{CO}, r_{OC}, r_{OB}, and r_{BO}) of the resulting closed–open–blocked (C↔O↔B) scheme were extracted by a simultaneous maximum likelihood fit to the dwell-time histograms of all conductance levels while accounting for the filter dead time (Csanády, 2000). Mean burst duration was then calculated as $(1/r_{OC})(1 + r_{OB}/r_{BO})$ (Figs. 1 F and 2 C), and mean interburst duration was calculated as $1/r_{CO}$ (Figs. 1 G and 2 D). The estimates of interburst duration, and consequently of channel open probability (P$_o$), are sensitive to correct estimation of the number of channels (N) in the patch. These parameters were therefore used only if N could be determined with reasonable confidence; for this subset of patches, N was ≤5.

To extract the gating pattern of channels loaded with either ATP or P-ATP at both sites, segments immediately following nucleotide exchange were not included in our analysis. The starting point for idealization was assigned individually for each patch, based on visual inspection, with analysis restricted to segments in which the gating pattern had already stabilized. The time required for stabilization after nucleotide exchange was typically between 10 and 60 s. To facilitate nucleotide loss from site 1, believed to happen faster in closed channels (Tsai et al., 2010), in some cases patches were rinsed with nucleotide-free solution for 20–30 s before applying a different nucleotide (e.g., Figs. 4 and 6).

Burst analysis of single-channel patches

Burst analysis was done as described previously (Csanády et al., 2010). In brief, open bursts from records with a single active channel were isolated by ignoring closures shorter than a cutoff, chosen using the method of Jackson et al. (1983). The distributions of the durations of bursts obtained in this way were fitted using maximum likelihood (Colquhoun and Sigworth, 1995) to either a single-exponential distribution (Fig. 7, A and B, blue dotted lines) or to the scheme in Fig. 7 C, with the slow rate k_1 fixed to 0 (Fig. 7, A and B, red solid lines); events shorter than t_{low} = 12

ms were excluded from the analysis. The probability density functions of the two fitted models are given by $f(k, t) = k \cdot \exp(-kt)$ and $f(k_1, k_2, t) = (k_1 k_2/(k_2 - k_1)) \cdot (\exp(-k_1 t) - \exp(-k_2 t))$, respectively; the improvement of the fit caused by introduction of the second free parameter was evaluated using the log-likelihood ratio test and found significant for both distributions in Fig. 7 (A and B).

Analysis of macroscopic current relaxations

Macroscopic current decay time courses were fitted with single-exponential functions using nonlinear least squares (pClamp9), and the closing rate was defined as the inverse of the fitted time constant. For the nonhydrolytic mutants (K1250A, E1371S, and double mutants), the decay time courses after nucleotide removal often required a double-exponential function—of the form I(t) = I$_0$(A$_1$exp($-t/\tau_1$) + (1 − A$_1$)exp($-t/\tau_2$))—with two slow time constants for a satisfactory fit (e.g., Fig. 3, B and E), suggesting the presence of two populations of open-channel bursts. In such cases, the average steady-state burst duration (τ^*) was estimated as $\tau^* = \tau_1\tau_2/(A_1\tau_2 + A_2\tau_1)$, and the average closing rate was defined as $1/\tau^*$ (Szollosi et al., 2011).

Mutant cycle analysis

Mutant cycle analysis (Fersht, 2002) was used to give a measure of the energetic coupling ($\Delta\Delta G_{int}$) between pairs of target structural elements, as described previously (Vergani et al., 2005; Szollosi et al., 2010, 2011). In brief, perturbation-induced changes (between corners i and j of a mutant cycle) in activation free energy barriers ($\Delta\Delta G^{\ddagger}$) for closing were calculated from the changes in (hydrolytic and nonhydrolytic) closing rates (r) as $\Delta\Delta G^{\ddagger}_{j-i} = -RT ln(r_j/r_i)$, and $\Delta\Delta G_{int}$ was defined as the difference between $\Delta\Delta G^{\ddagger}$ values along parallel sides of the mutant cycle (e.g., $\Delta\Delta G^{\ddagger}_{4-3} - \Delta\Delta G^{\ddagger}_{2-1}$). All ΔGs are given as mean ± SEM. Because the numbers of observations, n, for each corner of the cycle are similar, SEMs were calculated using the mean value for n.

Statistics

Data are given as mean ± SEM of at least five measurements. Statistical significance was evaluated using Student's t test (*, P < 0.05; **, P < 0.01).

Online supplemental material

Fig. S1 compares single-channel conductances in ATP versus P-ATP. Fig. S2 shows the effect of the K464A mutation on nonhydrolytic closing rate measured in the E1371S background. Figs. S1 and S2 are available at http://www.jgp.org/cgi/content/full/jgp .201210954/DC1.

RESULTS

P-ATP stimulates CFTR channel opening with high affinity and prolongs steady-state burst durations

We first determined rough kinetic parameters for CFTR channels gating in P-ATP in our experimental system. Apparent affinities for ATP and P-ATP were compared in macroscopic patches by applying test concentrations of the nucleotide bracketed by applications of a saturating (2 mM and 32 µM, respectively) concentration (Fig. 1, A and B). Fractional currents plotted against nucleotide concentration (Fig. 1 C) were well fit by the Michaelis–Menten equation and yielded K$_m$ values of 40 ± 2 µM for ATP but 2.4 ± 0.2 µM for P-ATP (Fig. 1 C, blue and red). We next compared steady-state gating of CFTR channels exposed either to a close-to-saturating
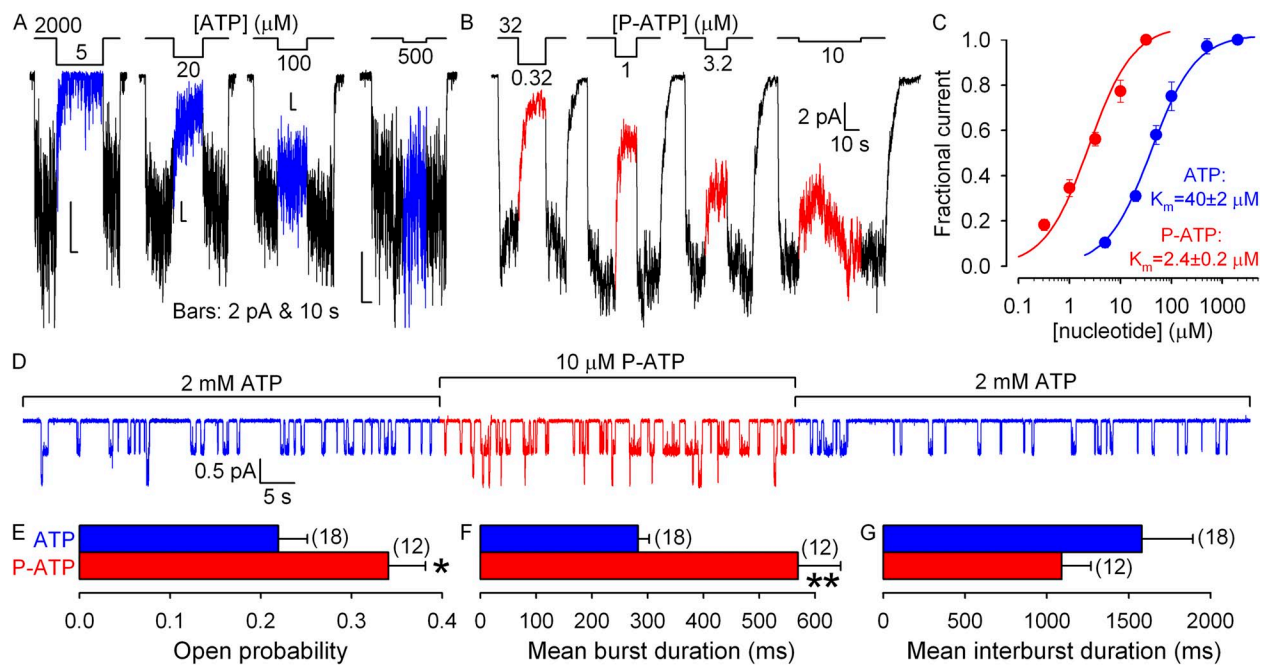
Figure 1. Effects of P-ATP on rough channel gating parameters of WT CFTR. (A and B) Macroscopic currents of prephosphorylated CFTR channels elicited by step applications (bars) of various concentrations of ATP (A) or P-ATP (B). (C) Dose–response curves for current stimulation by ATP (blue symbols) and P-ATP (red symbols). Mean steady currents in the presence of test nucleotide concentrations were normalized to the average of those measured in bracketing segments in the presence of 2 mM (ATP) or 32 µM (P-ATP) nucleotide. Fits to the Michaelis–Menten equation (solid lines) yielded K_m values shown. (D) Steady-state current recording from a patch containing two active WT CFTR channels gating in 2 mM ATP (blue segments) or 10 µM P-ATP (red segment). (E–G) Steady-state open probabilities (E), mean burst durations (F), and mean interburst durations (G) of WT CFTR in the presence of 2 mM ATP (blue bars) or 10 µM P-ATP (red bars), extracted from records with ≤2 active channels, as described in Materials and methods.

concentration of 10 µM P-ATP or to 2 mM ATP, in patches containing a few (≤2) channels in which individual gating transitions remained clearly resolved (Fig. 1 D). Kinetic analysis (see Materials and methods) revealed significantly higher P_o in P-ATP as compared with that seen in ATP (Fig. 1 E), which was largely caused by approximately twofold longer mean burst durations (Fig. 1 F) together with a small reduction in interburst durations (Fig. 1 G). These results confirm

earlier studies that have established P-ATP as a high affinity, potent CFTR stimulator (Zhou et al., 2005; Tsai et al., 2010).

[ATP] does not affect the prolongation of steady-state burst duration by the H1348A mutation

In an earlier study, we found that the H1348A mutation prolongs burst durations of CFTR channels gating in 2 mM ATP by approximately threefold (Szollosi et al., 2011).
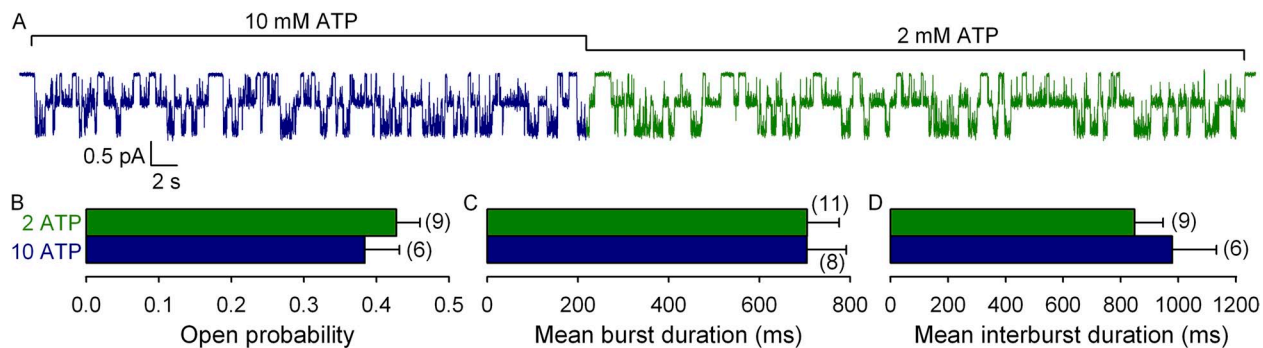

Figure 2. Steady-state mean burst duration of H1348A CFTR is insensitive to elevation of [ATP]. (A) Steady-state current recording from a patch containing two active H1348A CFTR channels gating in 2 mM (green segment) or 10 mM (dark blue segment) ATP. (B–D) Steady-state open probabilities (B), mean burst durations (C), and mean interburst durations (D) of H1348A CFTR in the presence of 2 mM (green bars) or 10 mM (dark blue bars) ATP, extracted from records with ≤5 active channels, as described in Materials and methods.

Because for another site-1 mutant (W401F) mean burst durations were shown to increase at high millimolar ATP concentrations (Jih et al., 2012b), we tested whether that was the case for H1348A CFTR. However, comparing the patterns of gating in 2 and 10 mM ATP (Fig. 2 A) did not reveal any significant effect of raising [ATP] above 2 mM; kinetic analysis revealed identical P_o (Fig. 2 B), mean burst (Fig. 2 C), and interburst (Fig. 2 D) durations under these two conditions.

Both P-ATP and the H1348A mutation slow nonhydrolytic channel closure

To quantitatively compare the effects of our site-1 perturbations on the slow rate of nonhydrolytic closure, we studied macroscopic closing rates after nucleotide removal for channels in which nucleotide hydrolysis at site 2 is abrogated by mutagenesis. Because different NBD2 mutations, in addition to disrupting ATP hydrolysis, likely differentially alter the stability of the open state, we do not know which nonhydrolytic mutant is the best model for the O_1 state of WT CFTR. We therefore compared the effects of our site-1 perturbations on the closing rates of two nonhydrolytic mutants, NBD2 Walker A mutant K1250A (Fig. 3, A–C) and NBD2 Walker B mutant E1371S (Fig. 3, D–F). Both P-ATP (Fig. 3, A and D, red fit lines and time constants) and the H1348A mutation (Fig. 3, B and E, green fit lines and time constants) caused markedly slower current relaxations than those observed for the two background constructs upon removal of ATP (Fig. 3, A and D, blue fit lines and time constants; cf. Zhou et al., 2005; Szollosi et al., 2011). Thus, the nonhydrolytic closing rate (Fig. 3, C and F, bars; calculated from the fitted relaxation time constants as described in Materials and methods) was similarly affected by both site-1 perturbations, and this was true regardless of whether the K1250A (Fig. 3 C) or the E1371S (Fig. 3 F) mutant was chosen as the nonhydrolytic model; i.e., both site-1 perturbations decreased this rate by two- to threefold.

Nonadditive effects of P-ATP and site-1 mutations on hydrolytic closure support slowing of this gating step by P-ATP bound in site 1

The slowing of both hydrolytic and nonhydrolytic closure by P-ATP was suggested to result from occupation of site 1 by this nucleotide, based on the delayed onset of both effects upon application of the analogue (Tsai et al., 2010). We used thermodynamic mutant cycles (Fersht, 2002) as an independent approach to test this hypothesis. Nonadditive effects on gating of two structural perturbations suggest that those two structural elements are energetically coupled. Channels opened by
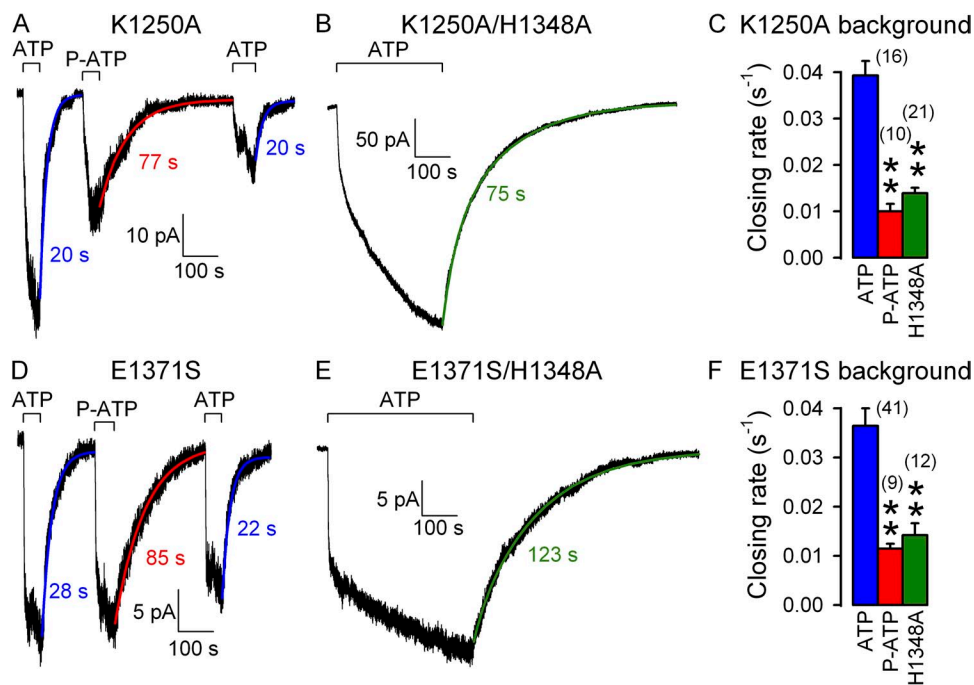
Figure 3. P-ATP and the H1348A mutation slow nonhydrolytic CFTR closure. (A and D) Macroscopic currents of prephosphorylated K1250A (A) and E1371S (D) CFTR channels elicited by exposure (bars) to either 10 mM ATP alternating with 50 µM P-ATP (A) or 2 mM ATP alternating with 10 µM P-ATP (D); the fivefold higher nucleotide concentrations for the K1250A constructs were used to compensate for the large decrease in apparent ATP affinity caused by this mutation (Vergani et al., 2003). Current decay time courses after sudden removal of the nucleotide were fitted with single exponentials (colored solid lines); colored numbers are time constants (in milliseconds), which reflect mean burst durations. (B and E) Macroscopic currents of prephosphorylated K1250A/H1348A (B) and E1371S/H1348A (E) CFTR channels elicited by transient exposure (bars) to either 10 mM (B) or 2 mM (E) ATP. Current decay time courses after sudden ATP removal were fitted with double exponentials (colored solid lines); colored numbers are calculated average burst durations (τ*, in milliseconds; see Materials and methods). The fit parameters were $\tau_1 = 37$ s, $\tau_2 = 165$ s, $A_1 = 0.34$, and $A_2 = 0.66$ for B, and $\tau_1 = 24$ s, $\tau_2 = 179$ s, $A_1 = 0.07$, and $A_2 = 0.93$ for E. (C and F) Nonhydrolytic closing rates of channels opened by ATP (blue bars) or P-ATP (red bars), or of channels bearing the H1348A mutation opened by ATP (green bars), measured in the K1250A (C) or E1371S (F) background. Closing rates were calculated as the inverse of the decay time constant after nucleotide removal; for traces that were not well fit by a single exponential, the average closing rate was calculated as $1/\tau^*$.

Csanády et al. 65

P-ATP contain two structural "perturbations": a phenyl-ethyl group (P group) linked to N^6 of the adenine of the nucleotide bound in site 1, and another P group on the nucleotide bound in site 2. If the presence of the P group in site 2 affects closing rate, then this effect is expected to be additive with effects on closing rate of mutations in the spatially distant site 1. In contrast, if the P group in site 1 is responsible for the effects of P-ATP on closing, then P-ATP and mutations of site-1 residues (which are energetically coupled to this P group) will affect closing rate in a nonadditive manner. We chose two site-1 perturbations to test for additivity of effects on closing rate with those of P-ATP. On the NBD2 side of site 1 we chose mutation H1348A, because this perturbation causes a large effect on closing rate in ATP, which we had already characterized (Fig. 2). To perturb the NBD1 side of site 1, we chose to delete most of a nonconserved insertion in CFTR's NBD1 (called the "regulatory insertion" [RI]; Lewis et al., 2004) by coexpression of CFTR segments 1–414 and 433–1480. This "ΔRI" perturbation leaves ATP-dependent

gating largely intact (Csanády et al., 2005) but is nevertheless expected to cause local distortion in areas of NBD1 that contact the adenine base of the site-1–bound nucleotide.

We first characterized the effect of P-ATP on hydrolytic closing rate in these two mutant backgrounds (Fig. 4) by recording single-channel activity of H1348A (Fig. 4 A), or of ΔRI channels (Fig. 4 D), alternately exposed to either 2 mM ATP (Fig. 4, A and D, green segments) or 10 µM P-ATP (Fig. 4, A and D, brown segments). Consistent with previous work, the H1348A and ΔRI perturbations differentially affected hydrolytic closure: the closing rate in ATP was unchanged for ΔRI (Fig. 4 E; compare green bar with blue bar; cf. Csanády et al., 2005), but two- to threefold slowed for H1348A (Fig. 4 B; compare green bar with blue bar; cf. Fig. 2 C). However, switching from ATP to P-ATP (Fig. 4, A and D, brown segments) did not elicit any noticeable change in the length of channel open bursts for either construct (Fig. 4, A and D; compare brown with green segments in expanded insets). Thus, P-ATP does not slow
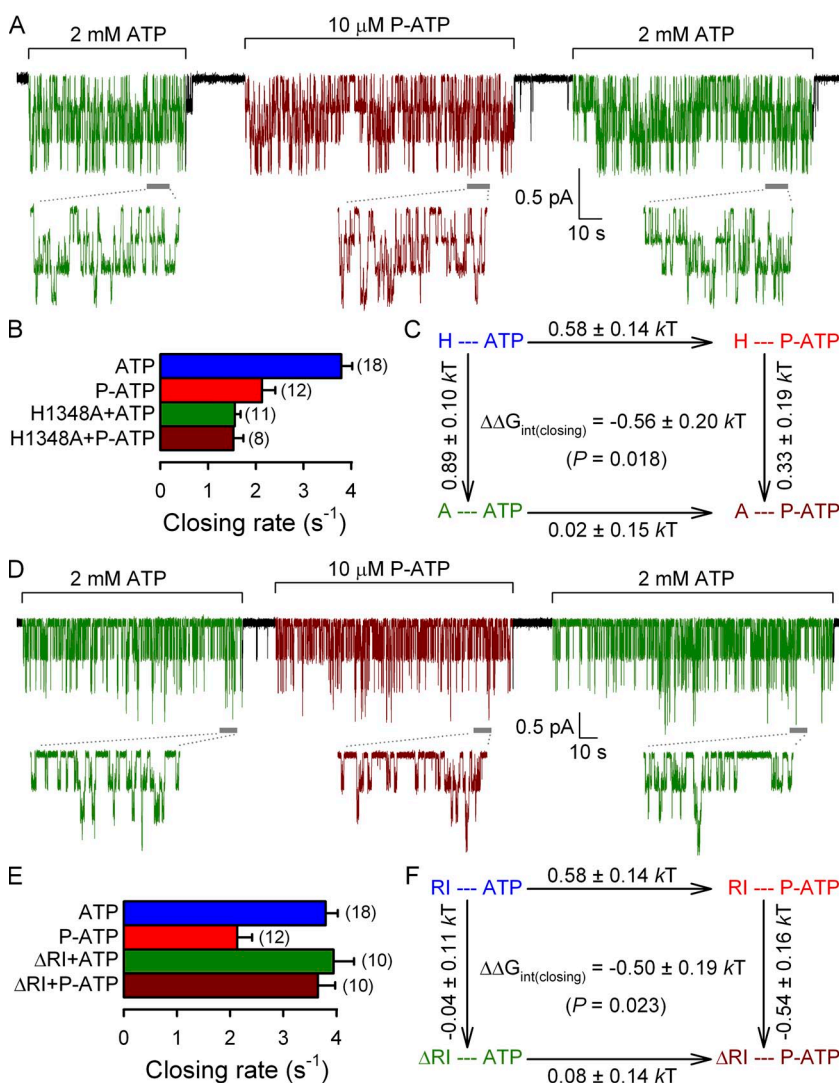
Figure 4. Mutation H1348A and deletion of segment 415–432 (ΔRI) abolish the effect of P-ATP on hydrolytic channel closure. (A and D) Steady-state recordings of single-channel currents in the presence of 2 mM ATP (green segments) or 10 µM P-ATP (brown segments) for H1348A (A) or ΔRI CFTR (D). Insets show at an expanded time scale 10-s intervals taken from the stable steady section of each segment (gray bars). In A, V_m was −40 mV. (B and E) Closing rates, obtained as the inverses of the steady-state mean burst duration, for H1348A (B) and ΔRI (E) CFTR channels gating in ATP (green bars) or P-ATP (brown bars). Steady-state closing rates of WT CFTR in ATP (blue bars) and P-ATP (red bars) were extracted from the data shown in Fig. 1 F. (C and F) Thermodynamic mutant cycles built on (hydrolytic) closing rates for the interaction of the P-ATP P group with residue 1348 (C) or the RI region (F). Each corner is represented by the particular site-1 protein structure (H or A at position 1348 [C]; maintained or deleted RI [F]) and the nucleotide driving gating (ATP or P-ATP), respectively. $\Delta\Delta G^\ddagger$ values (mean ± SEM) on arrows show perturbation-induced changes in the stability of the closing transition state with respect to the open ground state and were used to calculate (see Materials and methods) the coupling energy for the P group–1348 (C) and the P group–RI (F) interaction ($\Delta\Delta G_{int(closing)}$).

hydrolytic closure when applied in the H1348A or ΔRI mutant background (Fig. 4, B and E; compare brown with green bars). Although the twofold effect of P-ATP on hydrolytic closing rate of WT CFTR is small in energetic terms, the difference in the effects of the mutations on closing rates in P-ATP versus those in ATP yielded interaction free energies ($\Delta\Delta G_{int(closing)}$)—both between the P group and residue 1348 (Fig. 4 C) and between the P group and the RI region (Fig. 4 F)— which were significantly different from zero (P < 0.05). This is consistent with the effect on hydrolytic closing rate being caused by the P group in site 1.

Nonadditive effects of P-ATP and site-1 mutations on nonhydrolytic closure support the slowing of this gating step by P-ATP bound in site 1

Additivity of effects on nonhydrolytic closure of the same site-1 perturbations with those of P-ATP was tested in the K1250A nonhydrolytic background (Fig. 5) by measuring the macroscopic closing rate of K1250A/H1348A channels (Fig. 5 A), and of channels obtained by co-expression of segments 1–414 and 433–1480(K1250A) (K1250A/ΔRI; Fig. 5 D) upon nucleotide removal.

The H1348A and ΔRI perturbations affected nonhydrolytic closing rate in opposite ways; whereas mutation H1348A slowed it by approximately threefold (Fig. 5 B; compare green bar with blue bar; cf. Fig. 3 C), the ΔRI perturbation accelerated it by approximately threefold (Fig. 5 E; compare green bar with blue bar; cf. Csanády et al., 2005). Interestingly, neither perturbation abolished the effect of P-ATP on nonhydrolytic closure (Fig. 5, A and D; compare brown with green single-exponential fit lines and time constants); rather, both perturbations seemed to potentiate it. Thus, whereas P-ATP slowed nonhydrolytic closure by approximately fourfold for K1250A channels with an intact site 1 (Fig. 3 C; compare red with blue bar; replotted in Fig. 5, B and E), this effect increased to greater than sixfold and to approximately ninefold, respectively, in the presence of the site-1 perturbations H1348A and ΔRI (Fig. 5, B and E; compare brown with green bars), again suggesting nonadditivity. Indeed, mutant cycles built on nonhydrolytic closing rates (Fig. 5, C and F) yielded interaction free energies between the P group and residue 1348 (Fig. 5 C), as well as between the P group and the RI region (Fig. 5 F), significantly different from zero (P < 0.05
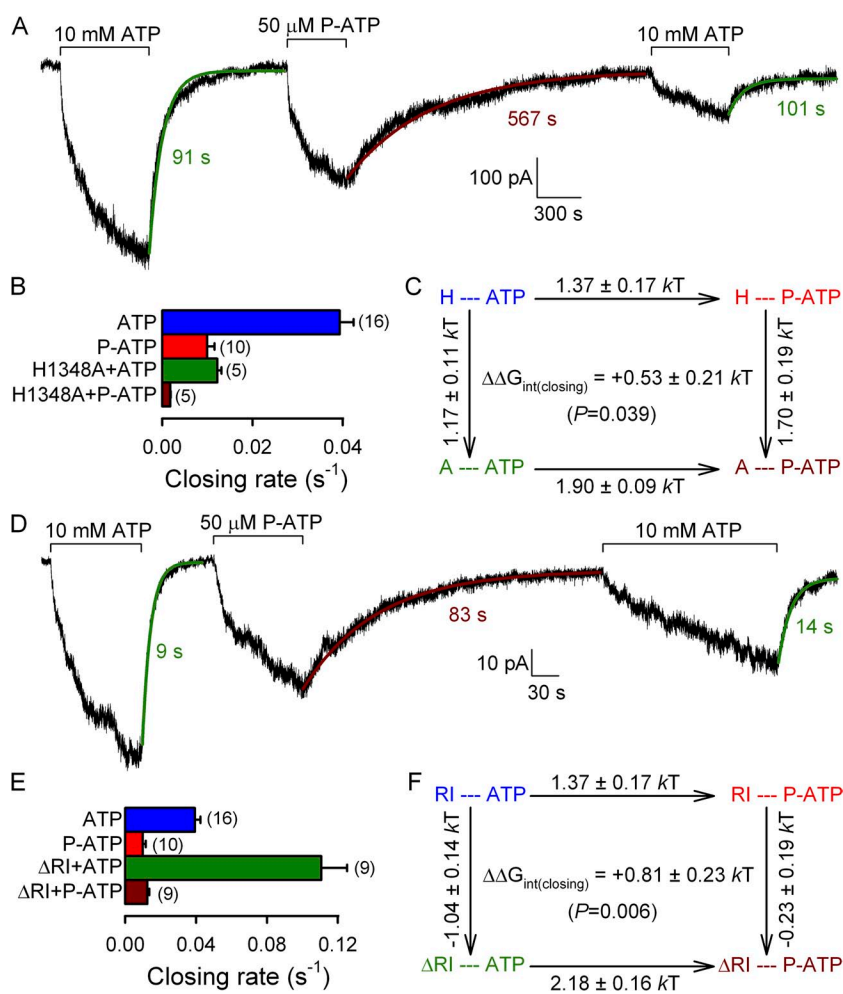

Figure 5. Mutation H1348A and deletion of segment 415–432 (ΔRI) potentiate the effect of P-ATP on nonhydrolytic channel closure. (A and D) Macroscopic currents from K1250A/H1348A (A) and K1250A/ΔRI (D) CFTR channels elicited by exposures to 10 mM ATP or 50 μM P-ATP (bars). Solid lines are single-exponential fits to the current relaxation time courses upon nucleotide removal, with time constants indicated. (B and E) Nonhydrolytic closing rates for K1250A/H1348A (B) and K1250A/ΔRI (E) CFTR channels, obtained as the inverses of the relaxation time constants upon removal of ATP (green bars) or P-ATP (brown bars); closing rates of K1250A CFTR upon removal of ATP (blue bars) and P-ATP (red bars) were replotted from Fig. 3 C. (C and F) Thermodynamic mutant cycles built on nonhydrolytic closing rates for the interaction of the P-ATP P group with residue 1348 (C) or the RI region (F). Each corner is represented by the particular site-1 protein structure (H or A at position 1348 [C]; maintained or deleted RI [F]) and the nucleotide driving gating (ATP or P-ATP), respectively. $\Delta\Delta G^{\ddagger}$ values (mean ± SEM) on arrows show perturbation-induced changes in the stability of the transition state for nonhydrolytic closure with respect to the open ground state and were used to calculate the coupling energy for the P group–1348 (C) and the P group–RI (F) interaction ($\Delta\Delta G_{int(closing)}$).

and P < 0.01, respectively), consistent with the effect on nonhydrolytic closing rate also being caused by the P group in site 1.

Neither P-ATP nor the H1348A mutation disrupts near 1:1 stoichiometry between ATP occlusion and channel burst events

Both P-ATP and the H1348A mutation prolong steady-state mean burst durations (Figs. 1 F and 2 C). Recent studies suggested a novel mechanism for a prolongation of steady-state CFTR burst durations for NBD1 mutant W401F (Jih et al., 2012a,b), by proposing the presence of a short time window at the end of each burst during which the hydrolysis products ADP and phosphate at site 2 can be replaced by a new ATP molecule without intervening channel gate closure. Such a "reentry" mechanism should allow for more than one ATP hydrolysis cycle to happen within a single

burst, thereby prolonging the mean duration of bursts at steady state. A simply testable prediction of such a model is a discrepancy between the burst durations measured at steady state and the time constant of the macroscopic current relaxation upon sudden removal of ATP. This is because the latter closing rate is measured under conditions that preclude a reentry cycle, i.e., in the absence of nucleotides. Because the W401F mutation also resides in site 1, we asked whether a reentry mechanism might explain the longer burst durations in P-ATP or in the presence of the H1348A mutation. To this end, we measured macroscopic closing rates after nucleotide removal for WT and ΔRI channels opened by either 2 mM ATP or by 10 µM P-ATP (Fig. 6, A and C), and for H1348A channels opened by 2 or 10 mM ATP (Fig. 6 B, top) or by 10 µM P-ATP (Fig. 6 B, bottom). Current relaxation time courses were fitted by single exponentials (Fig. 6, A–C, colored
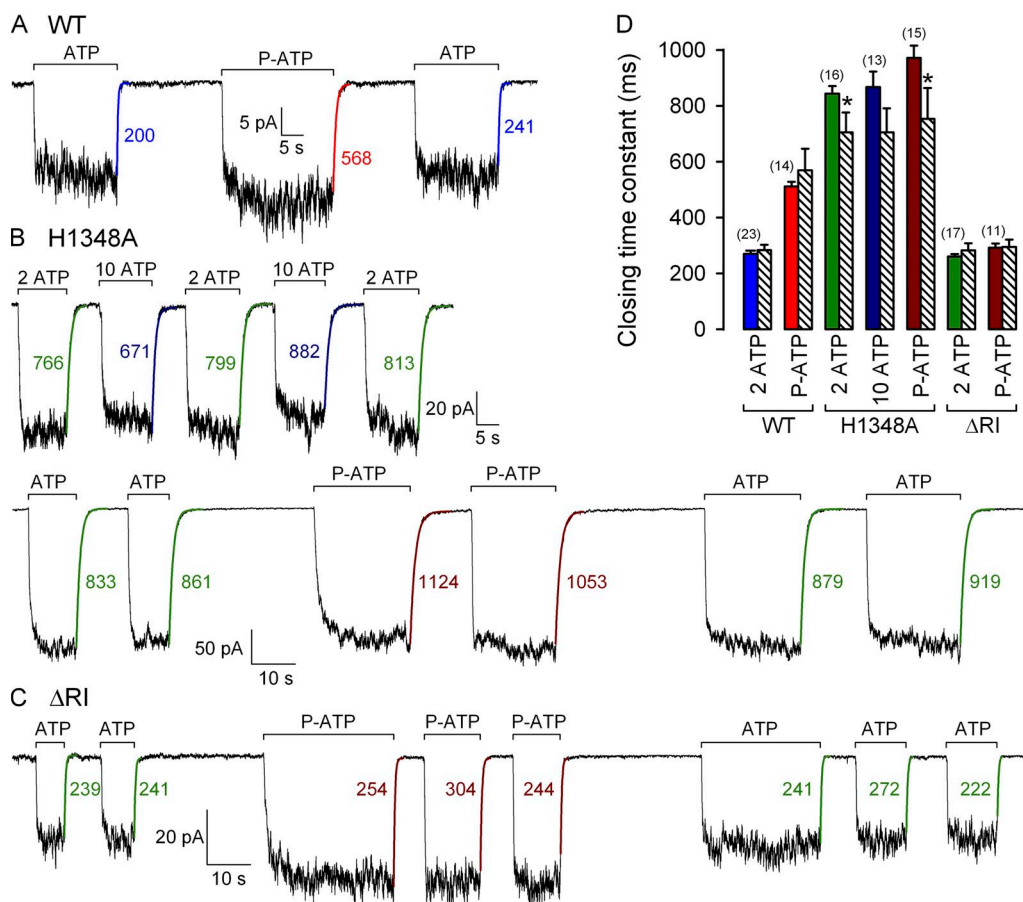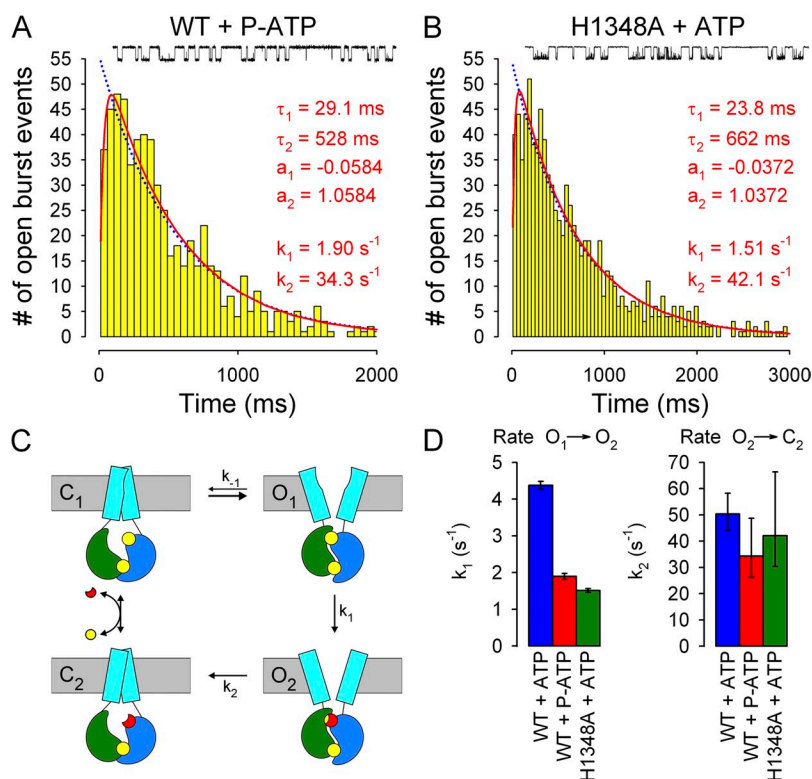

Figure 6. Relaxation time courses of macroscopic WT, H1348A, and ΔRI CFTR currents upon sudden nucleotide removal. (A–C) Macroscopic currents of prephosphorylated WT (A), H1348A (B), and ΔRI (C) CFTR channels elicited by exposure (bars) to either 2 mM ATP alternating with 10 µM P-ATP (A and C), or 2 mM ATP alternating with either 10 mM ATP (B, top) or 10 µM P-ATP (B, bottom). Current decay time courses upon sudden removal of the nucleotide were fitted with single exponentials (colored solid lines); colored numbers are time constants (in milliseconds). (D) Closing time constants of WT CFTR currents upon removal of 2 mM ATP (blue bar) or 10 µM P-ATP (red bar), of H1348A CFTR currents upon removal of 2 (left green bar) or 10 mM ATP (dark blue bar) or 10 µM P-ATP (left brown bar), and of ΔRI CFTR currents upon removal of 2 mM ATP (right green bar) or 10 µM P-ATP (right brown bar). As a comparison, striped bars replot mean burst durations of the respective constructs measured at steady state in the presence of the respective nucleotide (from Figs. 1 F, 2 C, and 4, B and E).

lines). The time constants of these exponentials reflect the mean duration of bursts, which do not contain reentry events. When we compared these time constants (Fig. 6 D, colored bars) with the steady-state mean burst durations measured in the presence of the respective nucleotide (Fig. 6 D, striped bars; data replotted from Figs. 1 F, 2 C, and 4, B and E), we found in each case a very close agreement; importantly, in no case was the steady-state burst duration longer than the macroscopic estimate. This suggests that both for WT (and ΔRI) channels gating in P-ATP, and for H1348A channels gating in 2 or 10 mM ATP or 10 µM P-ATP, each steady-state burst involves occlusion of a single nucleotide at site 2, just as suggested for WT channels gating in ATP (Csanády et al., 2010).

Of note, enhancement of macroscopic WT CFTR current by P-ATP, relative to ATP, was slightly smaller (<1.5-fold; see Fig. 6 A) than expected from the fractional increase in P_o ($\sim$1.55-fold; Fig. 1 E). This small discrepancy is accounted for by the slightly smaller average conductance of channels opened by P-ATP, which likely reflects rapid flickery closures not fully resolved at our recording bandwidth (Fig. S1). Thus, at −80 mV, average unitary current of open channels was −0.59 ± 0.01 pA (n = 6) in ATP but significantly (P < 0.01) smaller, −0.55 ± 0.01 pA (n = 6), in P-ATP.

Both P-ATP and the H1348A mutation prolong bursts by slowing the $O_1 \rightarrow O_2$ transition

Thus, under the conditions studied here, the duration of each open burst includes some time spent in a prehydrolytic open state (O_1; Fig. 7 C) in which a nucleoside triphosphate is occluded at site 2, followed by a shorter time interval in a less stable post-hydrolytic open state (O_2; Fig. 7 C). Because the rate (k_1) of nonhydrolytic closure (step $O_1 \rightarrow C_1$; Fig. 7 C) is very slow (see Fig. 3), the overall mean burst duration is mostly determined by the rates of the $O_1 \rightarrow O_2$ and $O_2 \rightarrow C_2$ transitions (k_1 and k_2; Fig. 7 C). The latter two rates can be estimated by fitting the scheme in Fig. 7 C to the distributions of open burst durations using maximum likelihood (Colquhoun and Sigworth, 1995). To determine which of these two rates is affected by P-ATP and the H1348A mutation, respectively, we recorded currents from patches containing a single active channel (Fig. 7, A and B, insets). Open burst events were isolated by burst analysis (see Materials and methods), pooled from several patches, and fitted by maximum likelihood. The histograms of burst durations were distinctly peaked for both WT channels gating in 10 µM P-ATP (Fig. 7 A) and H1348A channels gating in 2 mM ATP (Fig. 7 B), consistent with a non-equilibrium gating cycle that involves nucleotide

Figure 7. P-ATP and the H1348A mutation slow the $O_1 \rightarrow O_2$ transition of CFTR channels. (A and B) Histograms of open burst durations compiled from 621 open burst events of single WT CFTR channels gating in 10 µM P-ATP (A) and from 908 open burst events of single H1348A CFTR channels gating in 2 mM ATP (B). Both distributions were fitted by maximum likelihood to either a single exponential (blue dotted lines) or to the scheme in C, with rate k_1 fixed to zero (red lines); the latter fits proved significantly (P < 0.01 for A and P ≈ 0.05 for B) better by the log-likelihood ratio test. Fit parameters, as well as calculated time constants and fractional amplitudes of the exponential components of the fitted distributions, are plotted in both panels. (Insets) 30-s segments of single-channel recordings. (C) Simplified cyclic gating scheme (from Csanády et al., 2010) used for maximum likelihood fitting of open burst distributions, depicting closed and open states with either ATP (states C_1 and O_1) or ADP (states C_2 and O_2) bound at site 2. Pore opening/closure is assumed quasi-simultaneous with formation/disruption of the NBD dimer. Cyan rectangles, TMDs; green, NBD1; blue, NBD2; yellow, ATP; red, ADP. (D) Summary of rates k_1 and k_2 obtained from the fits in A and B for WT CFTR gating in 10 µM P-ATP (red bars) and H1348A CFTR gating in 2 mM ATP (green bars); as a comparison, the values measured for WT CFTR gating in 2 mM ATP (blue bars) are replotted from Csanády et al. (2010). Error bars represent 0.5-unit log-likelihood intervals. Note that in the presence of the site-1 perturbations, rate k_2 could be estimated only to a limited precision because of the increased discrepancy between the values of k_1 and k_2 (compare Csanády, 2006; k_2/k_1 is 11, 18, and 29, respectively, for WT+ATP, WT+P-ATP, and H1348A+ATP).

hydrolysis. The most striking difference between these distributions and that found earlier for WT channels gating in ATP (Csanády et al., 2010) was in the tail, which was distinctly longer in the presence of the site-1 perturbations, whereas the positions of the peaks were little moved. Accordingly, the maximum likelihood fit yielded two- to threefold slower k_1 values (Fig. 7 D, left) in the presence of P-ATP (red bar) or the H1348A mutation (green bar) compared with the earlier estimate for WT channels gating in ATP (blue bar; replotted from Csanády et al., 2010). In contrast, neither P-ATP nor the H1348A mutation seemed to dramatically affect the faster rate k_2 (Fig. 7 D, right).

DISCUSSION

In this paper, we have investigated in detail the effects on channel gating of two structural perturbations at CFTR's degenerate interfacial ATP-binding site (site 1). The H1348A mutation removes a histidine side chain from the signature sequence of NBD2, thereby perturbing the NBD2 side of site 1, whereas the use of P-ATP introduces a phenylethyl group into this composite binding site. Although in our experiments, which involved prolonged exposure to P-ATP, both composite sites were presumably loaded with this ATP analogue, an elegant study by Tsai et al. (2010) convincingly demonstrated that the effect of P-ATP on burst length (compare Fig. 1 F) is caused by the P-ATP molecule bound at site 1, whereas P-ATP bound at site 2 is responsible for the high affinity, potent stimulation of opening rate (compare Fig. 1, B and C). In addition, experiments using the nonhydrolyzable ATP analogue AMPPNP together with P-ATP to lock WT channels in the open state suggested that the slowing of nonhydrolytic closure by P-ATP is also attributable to P-ATP bound at site 1 (Zhou et al., 2005). Here, we provide further independent support for this assignment by demonstrating nonadditive effects on both the hydrolytic and nonhydrolytic closing rate of P-ATP and of mutations on either face of composite site 1 (Figs. 4 and 5). Furthermore, combining maximum likelihood fitting of steady-state single-channel records with the analysis of macroscopic current relaxations, we have determined which microscopic rates are affected by these site-1 perturbations resulting in the increased stability of channel open states.

In two recent studies, Jih et al. (2012a,b) proposed the existence of a short time window at the end of each burst, which would follow the release of hydrolysis products from site 2 but precede gate closure, and allow a new ATP molecule to bind at site 2, returning the channel into a new prehydrolytic open state without intervening gate closure. They further proposed that mutations or pharmacological modulation might prolong CFTR channel bursts by increasing the frequency of such "reentry" events (Jih et al., 2012a,b; Jih and

Hwang, 2013). Because one such mutation (W401F) resides in site 1, we have evaluated the possibility that the H1348A mutation, or P-ATP bound in site 1, might also act by such a mechanism. However, the lack of effect of increasing [ATP] on steady-state burst durations of H1348A CFTR (Fig. 2 C) and the close agreement of macroscopic closing time constants upon nucleotide removal with steady-state mean burst durations (Fig. 6) ruled out this possibility and confirmed that the two site-1 perturbations studied here do not disrupt the near 1:1 stoichiometry between ATP occlusion events and pore opening events, characteristic to WT CFTR gating in ATP (Csanády et al., 2010). Although comparison of macroscopic and steady-state closing rates (Fig. 6) might not be sensitive enough to rule out slight deviations from 1:1 stoichiometry, it is clear that small effects would not be sufficient to explain the two- to threefold prolongation of burst durations by the H1348A mutation and P-ATP. We have therefore used a simplified cyclic scheme (Fig. 7 C) as a framework for interpreting our kinetic results and have dissected the effects of site-1 perturbations on the three rates that determine the stability of the open states: those of steps $O_1 \rightarrow O_2$, $O_1 \rightarrow C_1$, and $O_2 \rightarrow C_2$ (Fig. 7 C).

Interestingly, the detailed kinetic consequences of these two perturbations turned out to be very similar, amounting to a simultaneous two- to threefold decrease in the rates of steps $O_1 \rightarrow O_2$ and $O_1 \rightarrow C_1$. This phenotype affords a simple explanation in terms of the free energy profile of the CFTR gating cycle (Fig. 8, blue energy profile). For a structural perturbation that selectively stabilizes the O_1 state, relative to both states C_1 and O_2 (by $\delta \Delta G_{O1}$; Fig. 8, red energy profile), a simultaneous increase in the heights of the transition-state barriers for both step $O_1 \rightarrow O_2$ ($\Delta G^{\ddagger}_1$; Fig. 8) and step $O_1 \rightarrow C_1$ ($\Delta G^{\ddagger}_{-1}$) is expected (compare red and blue vertical double arrows in Fig. 8), resulting in slowed rates k_1 and k_1, as observed. In addition, the distortion of the energy profile, as drawn, also suggests a lower energy barrier for step $C_1 \rightarrow O_1$, predicting an increase in opening rate. Interestingly, this is exactly what we observed for the H1348A mutant, the opening rate of which is approximately twofold increased relative to WT (compare Fig. 2 D, green bar, with Fig. 1 G, blue bar). We also observed a more modest increase in WT opening rate in the presence of 10 µM (subsaturating) P-ATP (compare red with blue bar in Fig. 1 G), but interpretation of this small effect is limited by the fact that stimulation of opening rate by P-ATP has been mostly attributed to P-ATP bound at site 2 (Tsai et al., 2010).

From an energetic point of view, the effects of the site-1 perturbations we have studied are modest, on the order of ~1 kT. However, two facts have to be considered when interpreting these effects. First, the measured $\Delta \Delta G$ values by no means represent the overall energetic change of the site-1 structure between states

C_1 and O_1, or O_1 and O_2, but the change in environment of a single chemical moiety (the histidine side chain at position 1348 or the phenylethyl group of P-ATP in site 1) associated with those gating transitions. Second, our $\Delta\Delta G$ values reflect changes in barrier heights, which suggest larger changes between ground states (see Fig. 8); e.g., an $\sim$1-kT change in the barrier height for nonhydrolytic closure might be associated with a $\Delta\Delta G$ of $\sim$2 kT between states C_1 and O_1. (As a comparison, $\Delta\Delta G_{int}$ between C_1 and O_1 is $\sim$2 kT for residues 555 and 1246 on opposing faces of the active site 2, which completely separates during the $O_1 \rightarrow C_1$ transition [Vergani et al., 2005].)

What mechanistic insight can be gained from these observations? The recent suggestion that composite site 1 of CFTR does not separate upon channel closure (Tsai et al., 2010; Szollosi et al., 2011) has fostered a view of the degenerate site as a simple rigid scaffold, which does not participate in the functional movements of asymmetric ABC-C proteins (although this proposal has remained a matter of contention; Artur et al., 2011). Our present data are hard to reconcile with such an assignment. The fact that removal of the histidine side chain at position 1348 selectively stabilizes state O_1 relative to C_1 (Fig. 8) is most simply explained by postulating that in the WT channel, the environment of that histidine side chain is not identical in those two states. The similar effect of P-ATP bound at site 1 suggests that the phenylethyl group also experiences a change in environment during the $C_1 \leftrightarrow O_1$ transition. It follows then that significant movement is likely to take place at site 1 during the channel opening step, even if the composite site does not actually separate in a closed channel.

Furthermore, the selective energetic stabilization of state O_1 relative to O_2 (Fig. 8) by both perturbations implies that in a WT channel, the physico-chemical environment of the H1348A side chain, or of the phenylethyl group of a P-ATP molecule bound at site 1, experiences a significant change also during the $O_1 \rightarrow O_2$ transition, i.e., upon ATP hydrolysis at the active composite site 2. The implication is a significant movement in site 1 upon ATP hydrolysis at site 2: a classical allosteric effect. Interestingly, the K464A mutation, which perturbs site 1 by removing the conserved Walker A lysine, was also shown to affect the energetics of both of the $C_1 \leftrightarrow O_1$ and $O_1 \rightarrow O_2$ gating steps (Csanády et al., 2010), although in a different way: in this mutant, rate k_1 decreased approximately fourfold, whereas the rate of nonhydrolytic closure, in a K1250A mutant background, increased by $\sim$10-fold (this is also replicated in the E1371S background; Fig. S2). Thus, although the distortion of the energetic profile by the K464A mutation differs from that seen for the two perturbations studied here, the K464A result is again consistent with movements in site 1 occurring in both of the above gating steps.

In principle, we cannot exclude the possibility of a "static allosteric effect" as an alternative scenario to explain our results. That is, perturbations in site 1 might statically impose a slightly different overall conformation of the NBDs, which leads to altered transition rates associated with reactions and conformational changes occurring at the active site 2, without movements in site 1 during those transitions. However, such an interpretation is at odds with the generally accepted view of protein allostery. Thus, manipulations at one site in a protein (the "allosteric site") that affect conformational
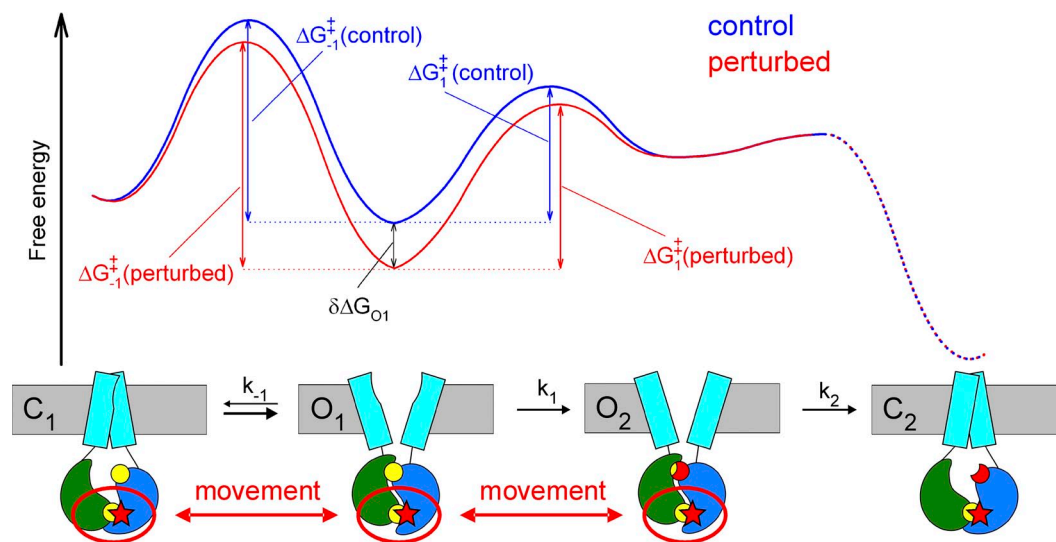

Figure 8. Energetic interpretation of the gating effects of P-ATP and the H1348A mutation. Free energy profiles (top; not drawn to scale) of channels moving sequentially through the gating states depicted below (from Fig. 7 C), in the absence (blue energy profile) or presence (red energy profile) of a perturbation (red star in cartooned states) in composite site 1. A selective stabilization of the O_1 ground state (by $\delta\Delta G_{O1}$, relative to both C_1 and O_2) is predicted to increase the heights of the free energy barriers for exiting O_1 in both directions ($\Delta G^{\ddagger}_{-1}$ and $\Delta G^{\ddagger}_{1}$; compare red and blue vertical double arrows), thereby slowing both rate k_1 and k_1 (cartoon).
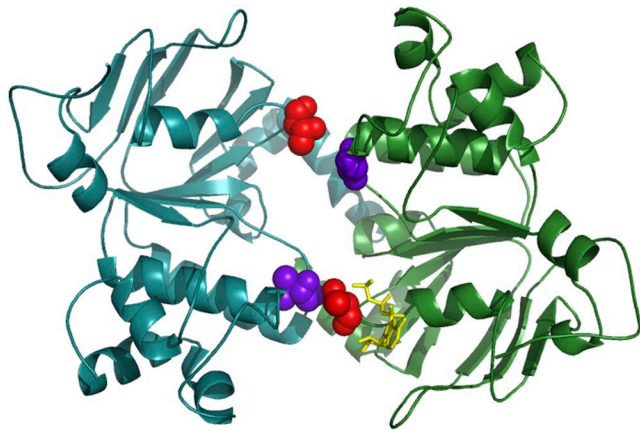
Figure 9. Partial separation of degenerate site in an asymmetrical bacterial ABC exporter. Ribbon diagram of NBD dimer from the crystal structure of TM287/288 (Protein Data Bank accession no. 3QF4), with AMPPNP (yellow) bound at the degenerate site. Conserved Walker A threonines (T368 in TM287 and T390 in TM288; red), as well as D-loop residue N521 of TM288 and corresponding TM287 residue S499 (violet), are highlighted in space fill. The empty active site is wide open, whereas the nucleotide-bound degenerate site retains some contact between the two NBD surfaces through opposing Walker A and D-loop motifs. NBD color coding follows that used in Fig. 7 C: green, TM287; blue, TM288.

changes at a distant site (the "active site") generally involve movement at the allosteric site itself: allosteric modulators affect the conformational equilibrium of proteins because the affinity of their binding sites changes during the conformational transition. Examples range from 2,3-bisphosphoglycerate or proton modulation of oxygen binding in hemoglobin (Monod et al., 1965) to activation of ligand-gated channels (Changeux and Edelstein, 2005); in contrast, we are not aware of any example of a "frozen" allosteric site. We therefore feel that a conventional "dynamic allosteric effect," which involves movements in site 1 of CFTR, is a more likely explanation of our findings.

Does site 1 separate then, or not, during a normal gating cycle? The answer might lie somewhere in between. The recent determination of the TM287/288 structure (Hohl et al., 2012) at least suggests such an intermediate scenario. In this structure, the TMDs are seen in an inward-facing orientation, generally believed to correspond to the closed-channel state in CFTR. At the same time, the NBD dimer interface is only partially separated (Fig. 9): the active site 2 is open and devoid of nucleotide (Fig. 9, top composite site), whereas the degenerate site (Fig. 9, bottom composite site) contains a bound AMPPNP molecule, and in it, the opposing faces remain in contact. In particular, the α-carbons of an asparagine in the TM288 D-loop (Asn521; Fig. 9, violet space fill) and that of a conserved threonine in the TM287 Walker A loop (T368; Fig. 9, red space fill) are separated by only 5.7 Å, and the asparagine is seen to make contact with the γ-phosphate of the bound

AMPPNP. Interestingly, the corresponding positions in site 1 of CFTR formed one of three interface pairs (T460-H1375) for which a lack of state-dependent changes in energetic coupling was interpreted to suggest a maintained interaction throughout the gating cycle (Szollosi et al., 2011). However, consistent with the data we present here, a comparison between TM287/288 and crystals with tightly dimerized NBDs highlights clear differences in composite site-1 structure. The distance between the Walker A motif and the opposing signature sequence of the degenerate site is larger by ∼3 Å in the TM287/288 structure (Hohl et al., 2012) than that seen in tight dimers of ABC NBDs (e.g., Smith et al., 2002; Dawson and Locher, 2007). The TM287/288 structure therefore also suggests some opening, although not complete separation, of the degenerate site.

In conclusion, the data presented here strongly suggest that significant movements occur in CFTR's composite site 1 concomitant with gating conformational changes. The precise extent and direction of these movements await further structural and functional studies.

REFERENCES

Aleksandrov, L., A.A. Aleksandrov, X.B. Chang, and J.R. Riordan. 2002. The first nucleotide binding domain of cystic fibrosis transmembrane conductance regulator is a site of stable nucleotide interaction, whereas the second is a site of rapid turnover. *J. Biol. Chem.* 277:15419–15425. http://dx.doi.org/10.1074/jbc.M111713200

Anderson, M.P., D.P. Rich, R.J. Gregory, A.E. Smith, and M.J. Welsh. 1991. Generation of cAMP-activated chloride currents by expression of CFTR. *Science.* 251:679–682. http://dx.doi.org/10.1126/science.1704151

Artur, L., P. Chaves, and D.C. Gadsby. 2011. Extent of nucleotide-binding domain (NBD) separation when a CFTR channel closes. *Biophys. J.* 100:265a–266a. http://dx.doi.org/10.1016/j.bpj.2010.12.1662

Basso, C., P. Vergani, A.C. Nairn, and D.C. Gadsby. 2003. Prolonged nonhydrolytic interaction of nucleotide with CFTR's NH$_2$-terminal nucleotide binding domain and its role in channel gating. *J. Gen. Physiol.* 122:333–348. http://dx.doi.org/10.1085/jgp.200308798

Cai, Z., T.S. Scott-Ward, and D.N. Sheppard. 2003. Voltage-dependent gating of the cystic fibrosis transmembrane conductance regulator Cl$^-$ channel. *J. Gen. Physiol.* 122:605–620. http://dx.doi.org/10.1085/jgp.200308921

Chan, K.W., L. Csanády, D. Seto-Young, A.C. Nairn, and D.C. Gadsby. 2000. Severed molecules functionally define the boundaries of the cystic fibrosis transmembrane conductance regulator's NH$_2$-terminal nucleotide binding domain. *J. Gen. Physiol.* 116:163–180. http://dx.doi.org/10.1085/jgp.116.2.163

Changeux, J.P., and S.J. Edelstein. 2005. Allosteric mechanisms of signal transduction. *Science.* 308:1424–1428. http://dx.doi.org/10.1126/science.1108595

Colquhoun, D., and F.J. Sigworth. 1995. Fitting and statistical analysis of single-channel records. *In* Single Channel Recording. Second edition. B. Sakmann and E. Neher, editors. Plenum Press, New York. 483–587.

Csanády, L. 2000. Rapid kinetic analysis of multichannel records by a simultaneous fit to all dwell-time histograms. *Biophys. J.* 78:785–799. http://dx.doi.org/10.1016/S0006-3495(00)76636-7

Csanády, L. 2006. Statistical evaluation of ion-channel gating models based on distributions of log-likelihood ratios. *Biophys. J.* 90: 3523–3545. http://dx.doi.org/10.1529/biophysj.105.075135

Csanády, L., K.W. Chan, D. Seto-Young, D.C. Kopsco, A.C. Nairn, and D.C. Gadsby. 2000. Severed channels probe regulation of gating of cystic fibrosis transmembrane conductance regulator by its cytoplasmic domains. *J. Gen. Physiol.* 116:477–500. http://dx.doi.org/10.1085/jgp.116.3.477

Csanády, L., K.W. Chan, A.C. Nairn, and D.C. Gadsby. 2005. Functional roles of nonconserved structural segments in CFTR's NH$_2$-terminal nucleotide binding domain. *J. Gen. Physiol.* 125:43–55. http://dx.doi.org/10.1085/jgp.200409174

Csanády, L., P. Vergani, and D.C. Gadsby. 2010. Strict coupling between CFTR's catalytic cycle and gating of its Cl- ion pore revealed by distributions of open channel burst durations. *Proc. Natl. Acad. Sci. USA.* 107:1241–1246. http://dx.doi.org/10.1073/pnas.0911061107

Dawson, R.J.P., and K.P. Locher. 2007. Structure of the multidrug ABC transporter Sav1866 from Staphylococcus aureus in complex with AMP-PNP. *FEBS Lett.* 581:935–938. http://dx.doi.org/10.1016/j.febslet.2007.01.073

Fersht, A. 2002. Structure and Mechanism in Protein Science. Fourth edition. W.H. Freeman and Company, New York. 650 pp.

Hohl, M., C. Briand, M.G. Grütter, and M.A. Seeger. 2012. Crystal structure of a heterodimeric ABC transporter in its inward-facing conformation. *Nat. Struct. Mol. Biol.* 19:395–402. http://dx.doi.org/10.1038/nsmb.2267

Hollenstein, K., R.J. Dawson, and K.P. Locher. 2007. Structure and mechanism of ABC transporter proteins. *Curr. Opin. Struct. Biol.* 17:412–418. http://dx.doi.org/10.1016/j.sbi.2007.07.003

Ishihara, H., and M.J. Welsh. 1997. Block by MOPS reveals a conformation change in the CFTR pore produced by ATP hydrolysis. *Am. J. Physiol.* 273:C1278–C1289.

Jackson, M.B., B.S. Wong, C.E. Morris, H. Lecar, and C.N. Christian. 1983. Successive openings of the same acetylcholine receptor channel are correlated in open time. *Biophys. J.* 42:109–114. http://dx.doi.org/10.1016/S0006-3495(83)84375-6

Jih, K.Y., and T.C. Hwang. 2013. Vx-770 potentiates CFTR function by promoting decoupling between the gating cycle and ATP hydrolysis cycle. *Proc. Natl. Acad. Sci. USA.* 110:4404–4409. http://dx.doi.org/10.1073/pnas.1215982110

Jih, K.Y., Y. Sohma, and T.C. Hwang. 2012a. Nonintegral stoichiometry in CFTR gating revealed by a pore-lining mutation. *J. Gen. Physiol.* 140:347–359. http://dx.doi.org/10.1085/jgp.201210834

Jih, K.Y., Y. Sohma, M. Li, and T.C. Hwang. 2012b. Identification of a novel post-hydrolytic state in CFTR gating. *J. Gen. Physiol.* 139:359–370. http://dx.doi.org/10.1085/jgp.201210789

Lewis, H.A., S.G. Buchanan, S.K. Burley, K. Conners, M. Dickey, M. Dorwart, R. Fowler, X. Gao, W.B. Guggino, W.A. Hendrickson, et al. 2004. Structure of nucleotide-binding domain 1 of the cystic fibrosis transmembrane conductance regulator. *EMBO J.* 23: 282–293. http://dx.doi.org/10.1038/sj.emboj.7600040

Monod, J., J. Wyman, and J.P. Changeux. 1965. On the nature of allosteric transitions: A plausible model. *J. Mol. Biol.* 12:88–118. http://dx.doi.org/10.1016/S0022-2836(65)80285-6

Procko, E., M.L. O'Mara, W.F.D. Bennett, D.P. Tieleman, and R. Gaudet. 2009. The mechanism of ABC transporters: general lessons from structural and functional studies of an antigenic peptide transporter. *FASEB J.* 23:1287–1302. http://dx.doi.org/10.1096/fj.08-121855

Riordan, J.R., J.M. Rommens, B. Kerem, N. Alon, R. Rozmahel, Z. Grzelczak, J. Zielenski, S. Lok, N. Plavsic, J.L. Chou, et al. 1989. Identification of the cystic fibrosis gene: cloning and characterization of complementary DNA. *Science.* 245:1066–1073. http://dx.doi.org/10.1126/science.2475911

Smith, P.C., N. Karpowich, L. Millen, J.E. Moody, J. Rosen, P.J. Thomas, and J.F. Hunt. 2002. ATP binding to the motor domain from an ABC transporter drives formation of a nucleotide sandwich dimer. *Mol. Cell.* 10:139–149. http://dx.doi.org/10.1016/S1097-2765(02)00576-2

Szollosi, A., P. Vergani, and L. Csanády. 2010. Involvement of F1296 and N1303 of CFTR in induced-fit conformational change in response to ATP binding at NBD2. *J. Gen. Physiol.* 136:407–423. http://dx.doi.org/10.1085/jgp.201010434

Szollosi, A., D.R. Muallem, L. Csanády, and P. Vergani. 2011. Mutant cycles at CFTR's non-canonical ATP-binding site support little interface separation during gating. *J. Gen. Physiol.* 137:549–562. http://dx.doi.org/10.1085/jgp.201110608

Tsai, M.F., M. Li, and T.C. Hwang. 2010. Stable ATP binding mediated by a partial NBD dimer of the CFTR chloride channel. *J. Gen. Physiol.* 135:399–414. http://dx.doi.org/10.1085/jgp.201010399

Vergani, P., A.C. Nairn, and D.C. Gadsby. 2003. On the mechanism of MgATP-dependent gating of CFTR Cl⁻ channels. *J. Gen. Physiol.* 121:17–36. http://dx.doi.org/10.1085/jgp.20028673

Vergani, P., S.W. Lockless, A.C. Nairn, and D.C. Gadsby. 2005. CFTR channel opening by ATP-driven tight dimerization of its nucleotide-binding domains. *Nature.* 433:876–880. http://dx.doi.org/10.1038/nature03313

Zhou, Z., X. Wang, M. Li, Y. Sohma, X. Zou, and T.C. Hwang. 2005. High affinity ATP/ADP analogues as new tools for studying CFTR gating. *J. Physiol.* 569:447–457. http://dx.doi.org/10.1113/jphysiol.2005.095083